Indutivo: Contact-Based, Object-Driven Interactions with Inductive Sensing

Jun Gong[1], Xin Yang[1,2], Teddy Seyed[3], Josh Urban Davis[1], Xing-Dong Yang[1]

Dartmouth College[1], Renmin University of China[2], University of Calgary[3]

{jun.gong.gr; josh.u.davis.gr; xing-dong.yang}@dartmouth.edu, teddy.seyed@ucalgary.ca

Figure 1. Indutivo recognizes the tap of a conductive objects on a smartwatch, such as (a) a dime, or (b) finger. It can sense (c) the rotation of a bottle cap instrumented using copper tape, (d) hinge of a metal credit card, and (e) slide of the handle of a table knife.

ABSTRACT

We present Indutivo, a contact-based inductive sensing technique for contextual interactions. Our technique recognizes conductive objects (metallic primarily) that are commonly found in households and daily environments, as well as their individual movements when placed against the sensor. These movements include sliding, hinging, and rotation. We describe our sensing principle and how we designed the size, shape, and layout of our sensor coils to optimize sensitivity, sensing range, recognition and tracking accuracy. Through several studies, we also demonstrated the performance of our proposed sensing technique in environments with varying levels of noise and interference conditions. We conclude by presenting demo applications on a smartwatch, as well as insights and lessons we learned from our experience.

Author Keywords

Wearable, smartwatch, inductive sensor

INTRODUCTION

Contextual interactions based on object recognition and manipulation have enormous potential in small wearable (e.g., smartwatches) or IoT devices (e.g., Amazon Echo, Nest Thermostat, Cortana Home Assistant), where input to these devices is generally difficult due to smaller form factors and the lack of effective input modalities [19, 31, 50, 56]. However, precise object recognition and lateral movement (e.g., slide, hinge and rotation) detection remains

challenging. For example, the existing technologies, such as RFID [23, 24] or electromagnetic-based [22, 49] approaches can detect and recognize objects but cannot sense object lateral movement precisely.

In this paper, we propose a new sensing technique based on induction, to enable contact-based precise detection, classification, and manipulation of conductive objects (primarily metallic) commonly found in households and offices (such as utensils or small electronic devices). Our technique allows a user to tap a conductive object or their finger on a device (e.g., a smartwatch) to trigger an action. Once the object is detected, the user can use it for continuous 1D input such as sliding, hinging, or rotating, depending on its physical affordance (Figure 1). With this technique, a context embedded item can be used to indicate a desired application followed by fluid continuous input without the need to switch input modalities.

Our prototype (called Indutivo) contains an array of five spiral-shaped coils, whose size, shape, and layout were carefully designed to balance sensitivity, sensing range, recognition and tracking accuracy. We developed the sensor in a smartwatch form factor with a software system and tested it using 23 daily objects that were a mix of conductive and non-conductive objects which were instrumented using low-cost copper tape, as well as a finger, in five everyday environments (e.g. office, living room). Results from ten participants showed a 95.8% real-time classification accuracy. Additionally, our study revealed that the system could track the slide of objects with an average error of 0.82 mm. It tracked an objects' hinge movement between 0° and 60° against the sensor with an average error of 1.6°. The system could also detect eight discrete rotational directions of an instrumented bottle cap, with a 93.3% accuracy. We also provide insights into the robustness of this approach under common environmental noises.

The contributions of this work include (1) a contact-based inductive sensing technique for recognizing conductive objects and tracking their lateral movements (e.g., slide,

hinge and rotation) for continuous input; (2) a series of studies evaluating the accuracy of our sensing technique under normal and noisy environments; and (3) several applications using a smartwatch form factor to demonstrate the unique interactions enabled by our technique.

RELATED WORK

Our work intersects with the following areas of research.

Object Identification and Motion Sensing

Wearable devices' built in sensors (e.g., accelerometer), were designed to detect the motion of the device to infer user activities (e.g., [5, 14]) instead of the motion of an input object. Many options exist for object recognition on devices like smartwatches even though most were developed for different computing platforms. RFID-based approaches are effective for object recognition, but the technology requires the object to be instrumented [6, 7, 17, 23, 24, 36, 43]. Capacitive NFCs [13] are similar, requiring the objects to be instrumented. Zanzibar [44] identifies instrumented objects place on its surface through NFC. Vision-based approaches can recognize tagged [9] or untagged objects [38] but camera-based approaches are power consuming.

There are also many sensing techniques that do not require object instrumentation. For example, acoustics-based approaches (e.g. [34, 46]) leverage acoustics to recognize objects that can make sound. EM-Sense [21] recognizes electrical objects via electromagnetic signals. ViBand [20] recognizes objects that generate mechanical or motor-powered vibrations. Radarcat [51] uses multi-channel radar signals to recognize electrical or non-electrical objects. Induction-based sensing techniques have also been used in object recognition. For example, Maekawa, et al. [26] used magnetic sensors and coils to recognize electrical objects. Wang, et al. [45] used magneto-inductive sensors to recognize electrical objects via electromagnetic radiation.

Our approach is different in that it recognizes conductive objects (electrical or not), and is also capable of sensing object lateral movement, an ability that has not been demonstrated using existing sensing techniques. We chose to explore the induction-based approach due to its promise in both object recognition and lateral movement sensing.

Input on Smartwatches

We demonstrate our sensing technique on a smartwatch to showcase its unique ability to enrich interactions on small wearable devices. Within the current research, input on smartwatches is accomplished primarily using touch. Since the touchscreen is small, input space outside the touchscreen has received substantial attention in research. Existing approaches include using the watch band [35], bezel [4], and the watch case [30] as a touchpad. Duet [8] extends the input space to joint-device interactions with a smartphone. Another major approach explores using the space near the smartwatch for input. For example, SkinTrack [54] and AuraSense [56] sense finger movements on the skin of the wrist. Skin buttons [19] has virtual touch buttons on the wrist

near the smartwatch. LumiWatch [47] integrates this work into a self-contained smartwatch implementation. Gesture Watch [18] uses proximity sensors to detect mid-air hand gestures above the touchscreen. Abracadabra [15] senses finger movements in and around the watch face.

Another body of related research focuses on input using fingers (e.g., pinch) [1, 10, 16, 25, 40, 52] or hand gestures (e.g., fist) [10, 11, 37, 52] from the same-side hand (e.g., the hand wearing the smartwatch). For example, GestureWrist [37] uses capacitive sensors to detect the changes in forearm shape to infer hand postures. Fukui, et al. [11] and Ortega-Avila et al. [32] achieved a similar set of gestures using an array of infrared photo reflectors placed inside the wristband. SensIR [27] uses a similar method but achieves significant improvements on accuracy and gesture quantity. WristFlex [10] and Tomo [52, 53] showed that sensing same-side hand postures can be achieved using force resisters or electrical impedance tomography (EIT) sensors. WristWhirl [12] senses input from wrist whirling using infrared proximity sensors on the watchband. Soli [25] detects in-air finger gestures based on optimized millimeter-wave radar.

One-dimensional continuous input can be sensed on a smartwatch using a digital crown. Recent commercial developments have also shown the success of a rotating bezel [2]. A research version of such an interface can be found in Pasquero, et al.'s work [33]. Xiao, et al. extended this idea by proposing twisting, tilting, and pushing the entire watch face when attached to a joystick-like mount [48]. Doppio [42] allows a user to use a second watch face as an input device that can be attached, hinged, or slid around a base watch face. We see that Indutivo can be a good addition to these existing techniques with its unique ability in object sensing and lateral movement detection for precise control.

INTERACTION TECHNIQUES

Users can interact with Indutivo using contact-based interactions (e.g., tapping, hinging, sliding, or rotating a conductive object) that have been previously studied and proven to be effective and usable [42]. We use a smartwatch as an example to demonstrate Indutivo interactions. In our current implementation, objects are required to be in contact with the sensor, primarily due to the relatively short sensing distance (see limitations about how to mitigate this).

Figure 2. Indutivo interactions.
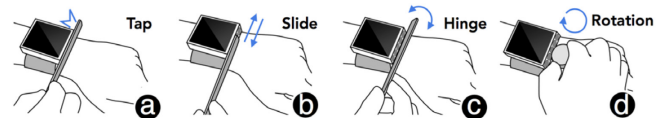
Tap. The user taps an object on the east side of the smartwatch (Figure 2a). The smartwatch recognizes the object and triggers an action. Tapping a different object triggers a different action. This can be used as a shortcut to quickly launch a user's favorite application. Tapping at different locations along the east side of the smartwatch can also trigger different actions.

Slide. Once recognized, a user can slide an object along the side of the watch for continuous 1D input (Figure 2b). It is a variation of Doppio's peek gesture, where the interaction is carried out on the side instead of on top of the touchscreen. The contact area of the object should be relatively planer in order to have control of the sliding movement.

Hinge. In addition to slide, the user can hinge a thin, flat object (e.g., the handle of a table knife) by rotating it along the edge of the smartwatch, visually resembling a hinged door (Figure 2c). Hinge also provides continuous 1D input, but in a different dimension, which increases the input space for different application needs.

Rotation. The user can also rotate a cylindrical object (e.g., a bottle cap or marker pen) against the side of the smartwatch, as if they were rotating a knob (Figure 2d). This is a variation of Doppio's stacked rotation, where the interaction is carried out on the side to avoid occluding the screen.

Environmental vs. Artificial Conductive Objective
We classify different types of conductive objects as either environmental or artificial. Environmental conductive objects are those that naturally occur in a user's home or office environment, such as a USB stick or table knife. Artificial conductive objects are objects instrumented using a conductive marker in the contact area (Figure 3). By pressing the marker to the sensor, the associated object can be recognized. This enabled us to increase the scope of recognition. We discovered that a simple way to create a conductive marker is to use a piece of copper tape. This works for both conductive and non-conductive objects. For example, instrumenting a book using a copper tape allows the book to be used as an input device (Figure 3a). Attaching the copper tape on a conductive object changes the inductance footprint of the object, creating a new input device using the same object (Figure 3b). Different patterns can be used to design the shape of the copper tape. This further increases the vocabulary of the conductive marker.
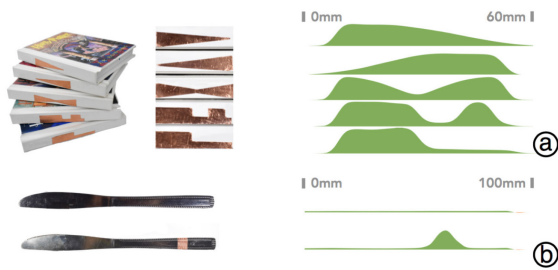
Figure 3. Left: (a) conductive markers created using copper tape. (b) table knives with and without instrumentation. Right: the inductive footprints of the corresponding objects (Y-axis shows raw sensor data on a scale from 0 to 3×10^7 in all figures).

SENSING PRINCIPLE
Inductive sensing is a sensing technology that enables low-cost, high-resolution sensing of conductive (mostly metallic) objects. Its sensing principle is based on Faraday's law of induction – a current-carrying conductor can "induce" a current to flow in a second conductor. More specifically, the

alternating electrical currents flowing through an inductor (e.g., a wound coil of the sensor) can generate an electromagnetic field. If a conductive object is brought into the vicinity of the inductor, the electromagnetic field will induce a circulating current (called an eddy current) on the surface of the target object. In turn, the induced eddy current will generate its own electromagnetic field, which opposes the original field generated by the inductor. As such, the sensor coil and the target form two coupled inductors, whose coupling affects the resonant frequency of the *L-C* resonator of the inductive sensor.

An important property of the resonant circuit is the ability to resonate at a specific frequency or resonant frequency (f_0), which can be described as a function of inductance (L) and capacitance (C) of the *L-C* resonator:

$$f_0 = \frac{1}{2\pi\sqrt{LC}} \qquad (1)$$

The effect of the field disturbance caused by approximating target object results in a shift of coil inductance, which can be observed as a shift in the resonant frequency. As both f_0 and C are known, the resulting inductance of the coil can be calculated using formula (1). The inductance of the sensor coil is affected by the resistivity, size, and shape of the target object and the distance between the sensor coil and target object. It is thus possible to infer the material (via resistivity), size, shape and distance of the target by measuring the resonant frequency of the L-C resonator.

Most conductive objects have capacitance and inductance, and both properties affect the resonant frequency. The effect of inductance dominates that of capacitance with most metallic objects. In contrast, the effect of capacitance becomes dominant with most non-metallic conductive objects, such as a finger. The latter was used in Touché [41] to distinguish between different ways a hand touches an instrumented household object.

Our system does not rely on capacitance for object recognition because capacitance is largely affected by the user's body, which acts like a big capacitor and diminishes the effect on capacitance caused by an object. As such, our technique works better with metallic objects (e.g., keys or utensils) or those mainly composed of metallic objects (e.g., electronic devices). Non-metallic conductive objects are mostly plant or food (e.g., fruits), and thus less suitable to be used for precise input. Our system can differentiate a finger from conductive objects due to the effects of capacitance and not inductance, again because the body acts as a capacitor.

HARDWARE IMPLEMENTATION
We created a prototype using customized hardware and software. This section presents our implementation details.

Coil Design
The key to the success of an inductive sensor is the design of the coils, as it affects the sensitivity, sensing range, recognition and tracking accuracy. The coils need to be placed along the side of a smartwatch, thus limiting our design to a rectangular region of approximately 10×40 mm

(e.g., approximately the size of a commercial smartwatch). Our design considers the following parameters: (1) coil shape, (2) coil size and arrangement, and (3) coil inductance.

Coil Shape. The coil needs to be spiraled with two ends connecting to the sensor. The shape of the coil mainly affects sensing distance, which is important for tracking the hinge movement. In principle, the coil can be made into any shape, but the most common are a square, hexagon, octagon, and circle (Figure 4). The circular coil has the best quality factor Q and lowest series resistance [3], allowing the largest possible sensing distance among the different options [28]. However, the tradeoff is that the sensor value of a circular coil is not as linearly proportional to the distance to the target as that of the other shapes, such as the rectangular coil. We chose the circular shape to maximize sensing distance.

Coil Size and Arrangement. In comparison to its shape, the physical size of the coil has an even larger effect on sensing distance [3]. Larger coils provide longer sensing distances. In our case, the diameter of the coils is limited by the height of a smartwatch, as well as the number of coils that are needed in the sensor. The size, shape, and lateral movement of an object against the sensor can be better sensed with an array of small but clustered coils (e.g., 3 × 15). However, hinge can be harder to detect with small coils, as our tests with several daily objects using the inductance to digital converter from TI (LDC1614) suggested that the maximum sensing distance of a circular coil is approximately 1 to 1.5 times its diameter. To balance the size and quantity of the coils, our final design used a linear array of five 7.39 mm coils with a 0.76 mm interval between each adjacent pair of the coils.
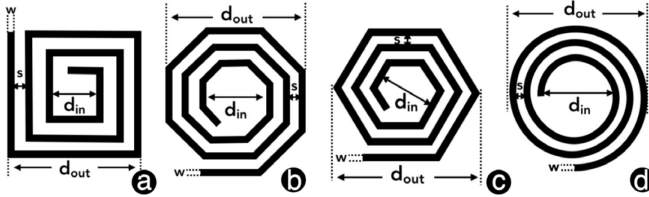

Figure 4. Four common designs of planar spiral coil: (a) square, (b) hexagon, (c) octagon, and (d) circle. *d_out* and *d_in* are outer and inner diameters respectively.

Coil Inductance. Unlike size and shape, coil inductance influences the intensity of the electromagnetic field, thus affecting sensor sensitivity to the small changes in the resonate frequency caused by objects of different materials, sizes, or shapes [3]. Figure 5 shows the relationship between coil inductance and the corresponding resonant frequency at a circuit capacitance value of 330 pF (suggested by Texas Instrument). It shows that small changes in the resonant frequency are more pronounced (e.g., steeper curve) with low inductances. In other words, the coil with a low inductance (or high resonant frequency) is preferred since it is more sensitive to the small shift in the resonant frequency.

Therefore, for each design solution, we calculated the corresponding inductance value and identify the one with the lowest inductance. The inductance of a singular layer of coil is determined by a number of parameters, such as number of
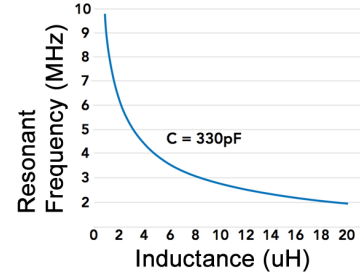
Figure 5. Resonant frequency shown by coil inductance.

turns or inner diameter, and can be calculated using the current sheet approximation formula [29]:

$$L_{single} = \frac{\mu n^2 d_{avg} c_1}{2} \left(\ln\left(\frac{c_2}{\rho}\right) + c_3 \rho + c_4 \rho^2 \right) \quad (2)$$

where

- μ is the permeability of free space, $4\pi \times 10^{-7}$
- n is the number of turns of the coil
- d_{avg} is the average diameter of the turns, which is defined as $(d_{out} + d_{in}) / 2$
- ρ represents the fill ratio of the coil, which is defined as $(d_{out} - d_{in}) / (d_{out} + d_{in})$
- c_i are geometry dependent parameters (for a circle, $c_1 = 1.0, c_2 = 2.46, c_3 = 0, c_4 = 0.2$)

For multi-layer coils, the total inductance of the coils in series can be calculated using the following formulas [39]:

$$L_{total} = \sum_{i=1}^{N} L_i + 2 \cdot \left(\sum_{j=1}^{N-1} \sum_{m=j+1}^{N} M_{j,m} \right) \quad (3)$$

where $M_{j,m}$ is the mutual inductance between the coils, which is defined as $k \cdot \sqrt{L_1 \cdot L_2}$. The parameter k is a measure of the flux linkage between the coils, whose value varies between 0 and 1. The value of k can be estimated using the formula proposed by Jonsenser Zhao [55]:

$$k = \frac{n^2}{0.64*(1.67n^2 - 5.84n + 65)*(Ax^3 - Bx^2 + Cx + D)} \quad (4)$$

where x is the distance in millimeters between the two adjacent layers and n is the number of turns of the coil. A, B, C, D are four constant parameters with the value of 0.184, -0.525, 1.038, 1.001 respectively [55].

Prior to designing a coil to maximize resonant frequency, it is important to understand that the upper bound of the resonant frequency is often limited by the working range of the inductance to digital converter. For example, the LDC1614 from TI supports a maximum resonant frequency of 10 MHz. Additionally, the signal stability of the inductance to digital converter may also limit the maximum resonant frequency. For example, our tests found that the readings of the LDC1614 became unstable when the resonant frequency exceeded 5 MHz. Therefore, we limited our exploration to strictly 5MHz.

Considering that many PCB shops print coil traces in 6 mils (0.15mm) wide with a minimum 6 mil interval between two adjacent traces, only four designs satisfied our needs. Table

1 shows these designs, where d_{out} and d_{in} are the diameter and inner diameter of the coils and Turns are the number of circles. Amongst these designs, we picked one that had the lowest inductance (shown in the first row).

d_{out} (mm)	d_{in} (mm)	Layers	Turns	Inductance (uH)	Frequency (MHz)
7.39	2.21	4	8	3.56	4.64
7.39	1.60	4	9	4.0	4.38
7.39	0.99	4	10	4.31	4.22
7.39	0.38	4	11	4.49	4.14

Table 1. Coil designs that satisfied our needs. The one highlighted in the first row was chosen.

Sensing Board

The coils are connected to two LDC1614 evaluation boards from Texas Instruments. Each board has a 28-bit inductance to digital converter (e.g., LDC1614) and a MSP430 microcontroller, used to interface the LDC1614 chip to a host computer. The LDC1614 chip has four output channels, one for each coil. It works by monitoring the resonant frequency of a L-C resonator and reports the corresponding inductance values. The sensing chip is developed to primarily respond to the inductance effect of a metallic object. As such, the capacitive effect of human body (e.g., hand flex) is neglectable. The system's sampling rate was set to 50Hz. According to datasheet, LDC1614 and coils consumes 10 mW when working and 0.1 mW in sleep mode. In our current implementation, the power consumption of each module is 103.8 mW, primarily from the MCU. The final prototype is shown in Figure 6.
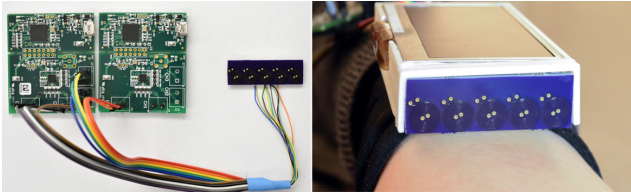
Figure 6. Left: LDC1614 evaluation boards and our custom-designed sensor coil. Right: Indutivo prototype.

OBJECT RECOGNITION & SENSING SLIDE, HINGE, AND ROTATION

Our prototype recognizes the contacted object and senses its manipulations (e.g., slide, hinge, or rotation), if any.

Object Recognition

Real-time object recognition was implemented by comparing the sensor data with a pre-collected database of labelled references. The closest match is used as the result.

Upon an object tapping anywhere on the sensor, the sensor reports a 1D array of five consecutive inductance values, one from each coil, representing the inductance footprint of the object (Figure 7 left). Aside from object material, the sensor data also encodes some low-resolution geometry information of the object's contact area (e.g., size and shape), which is also useful for recognizing objects. The reference footprint of an object is a scan of the object's contact area, composed of a curve representation of 1D continuous inductance values across the object's contact area, representing a high-resolution inductance footprint of the object (Figure 7 left).

Ideally, the scan can be carried out using a single coil and a tracking mechanism (e.g., VICON) precisely measuring the movement of the coil. This provides one-to-one mapping between a location inside the contact area and its corresponding inductance value. An alternative approach is to scan without tracking the position of the coil, which results in a similar curve, but on a different scale on the x-axis (e.g., time) caused by the speed of the coil movement. Assuming the coil is moved in a constant speed, the collected data can be converted from the time domain to the physical size domain using a scale factor $S = \frac{|t1 - t2|}{|d1 - d2|}$ if the corresponding coil locations (e.g., d_1 and d_2) of two randomly chosen times (e.g., t_1 and t_2) are known (e.g., measured manually). With this approach, testing and reference footprints can be compared in the same scale.
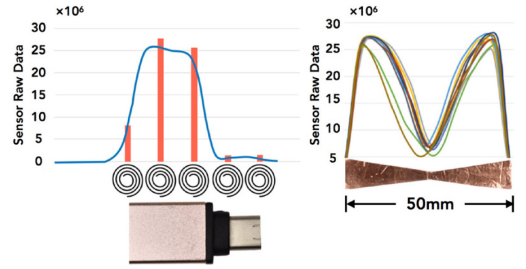
Figure 7. Left: inductance footprint of type-C adaptor shown in orange bars; reference footprint of the same object shown in blue. Right: ten scans of the reference footprint of Book 3.

We scanned the object by hand with the device wearing on the wrist. Since the consistency of the scanning speed cannot be guaranteed using the hand, we collected ten reference footprints for each object to accommodate the variance in scanning speed (Figure 7 Right). All reference footprints were scaled using the scale factor calculated based on the first scan. Naturally, scanning the object by hand creates errors in the resulting mapping between the inductance and the corresponding location in the object's contact area. However, our study revealed that such errors did not cause significant issues in recognizing objects and sensing the sliding movement. Finally, missing points between two adjacent samples in the reference footprint were interpreted linearly.

An important feature of the inductance footprint is encoding the length of the object's contact area through the span of the curve. However, such information is missing if the contact area is smaller than a coil (e.g., the barrel of the bottle cap), in which case, we scaled the footprint to match the diameter of the coil. While the length is no longer shown by the span of the curve, it is still reflected by the inductance value.

Before we compared a 5-pixel testing footprint with the references, we scaled them to the same scale. The final prediction was made using the k-nearest neighbors algorithm (KNN with k = 8), where for the testing footprint, we iterated

through all references in the database and calculated the smallest distance to each reference using:

$$\min_x \sum_{i=0}^{4} |f(x + d \times i) - y_i| \qquad (5)$$

where x is the location inside the object's contact area, d is the distance between two adjacent coils (e.g., 8.15 mm), y_i is the observed inductance value, and f is the reference footprint. The prediction result was made by majority voting based on the top eight candidates, ranked based on the similarity to the testing footprint. Once the object is identified, its location within the sensor is also known.

To maximize recognition accuracy, the object's contact area was required to be exposed to the sensor as much as possible. For example, the contact area needs to be inside the sensor if the object is smaller than the sensor. Otherwise, the sensor must be fully covered by the object. The object's contact surface should also be relatively planar, such that stable contact can be made against the sensor. How an object is in contact with the sensor may affect the geometry of the contact area, thus resulting in different inductance footprints. This enables new interactions but may cause ID collision. Despite these tradeoffs, the inductance footprint provides a reliable indication of different objects (see studies), making it possible to maintain a shared database of common objects.

Sensing Slide

After the object is tapped and predicted, its sliding movement can be detected by sensing the shift of the position of its corresponding reference footprint over the sensors (Figure 8). The center of the reference footprint of the object was used as the location of the object if: (1) it was smaller than the sensor or (2) the object itself was instrumented using copper tape. In the case of the object being larger than the sensor, sliding was carried out by tracking the movement of an end of that object (e.g., the end of the handle of a table knife). We set the northern end of the sensor to be the origin of the sensor's coordinate system (e.g., $x = 0$), which was manually specified for each object by tapping the object or its edge on the center of the northern most coil. For each of the ten reference footprints of the contacted object, we found its location over the sensor using:

$$\underset{x}{\text{argmin}}(\sum_{i=0}^{4} |f(x + d \times i) - y_i|) - x_0 \qquad (6)$$

where x_0 is the origin. The final prediction of the object's location is the average location of the top five candidates ranked based on the similarity to the testing footprint. The system supports both absolute and relative input.
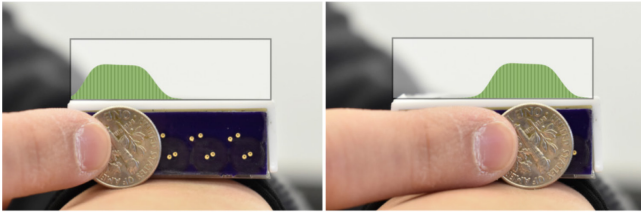
Figure 8. The position of the reference footprint indicates the position of the object inside the sensor.

Sensing Hinge

We developed a database of labelled references for sensing hinging angle by manually hinging open a flat object in a relatively constant speed, from 0° (e.g., object stands perpendicular to the wrist) to 60°. We did not go beyond 60° as it exceeds the sensing range for many objects. The collected data contains five inductance values, one from each coil and a corresponding time stamp. The data was then converted from the time domain to the hinging angle domain using a similar method described previously by using two reference hinging angles (e.g., 10° and 45°) measured manually using a protractor. For each object, we collected hinge movement data ten times.

When testing, the inductance values from the coils were used against the labelled data from each scan, where we found a local optimized prediction using:

$$\underset{x}{\text{argmin}} \sum_{i=0}^{4} |f_i(x) - y_i| \qquad (7)$$

where x is the hinging angle, f_i is the reference mapping collected from coil i, and y_i is the observed inductance value at coil i. The final prediction was the average angle of the top five candidates ranked based on similarity.

Similar to slide, hinge also works with both environmental and artificial conductive objects, but objects are required to be flat in order to provide a relatively stable hinging axis. Note that the location of the object inside the sensor is known, thus it is possible for users to trigger different actions by hinging at different locations. We only trained and tested hinge closer to the center of the sensor, but the reference data is independent of where it is collected, because the footprint can be shifted along the sensor coordinate. Slide and hinge can be uniquely identified via examining signal data. For example, with hinge, changes in the signal from different coils are similar (e.g. all increase) while signal from different coils changes sequentially with slide.

Sensing Rotation

Unlike slide and hinge, rotation only works with artificial conductive objects. To enable rotation, we placed a strip of copper tape along the barrel of a bottle cap. The width of the copper tape gradually increases to allow the sensor to pick up the cap's orientation based on the strength of the inductance signal. Our initial test suggested that this setup only works when the cap is rotated around a fixed axis, which cannot be guaranteed when using the hand. We thus decided to only support eight discrete levels (or wedges) of rotational directions using a staircase pattern, where each section is 12 mm long with a 1 mm increment (Figure 14 c). In this manner, each wedge on the cap was treated as an "object" in the reference database. Thus, detecting the rotation is simply detecting these "objects" using KNN.

EVALUATION 1 – OBJECT RECOGNITION

The goal of this study was to validate the object recognition accuracy of the proposed contact-based sensing approach, and its robustness across various locations as well as against individual variance among different users.

Participants

Ten right-handed participants (average age: 22.6, two female) were recruited to participate in this study. Participants wore the prototype on their left hand.

Objects

We tested 23 objects, classified into four types: large or small conductive objects and instrumented conductive or non-conductive objects (Figure 9). Large conductive objects are objects whose contact area is larger than the sensor. Some are metallic, while others are electronic devices with built-in metallic components. For small conductive objects, the contact area is smaller than the sensor. Instrumented conductive objects are conductive objects with a contact area instrumented using a strip of copper tape that is 10 mm wide. Instrumented non-conductive objects are non-conductive objects with the contact areas instrumented using copper tape with different patterns. Figure 9 also shows how an object is held against the sensor for both training and testing.

Study Procedure

One week prior to our study, references were collected with the sensor worn on the left hand by a volunteer and the system powered by a wall outlet (earth ground). We demonstrated to the volunteer which part of the objects to scan and how to scan in a relatively constant speed. No other instructions or training were given. Ten references were sampled for each object and the volunteer was not recruited again in our final study. The bottle cap was trained and tested using wedge 3, randomly picked from the eight options.

Prior to the start of the study, participants were briefly shown how to use each object. They understood that the object's contact area needed to be exposed to the sensor as much as possible. No practice trial was given. The study protocol is similar to the one used in [20, 49], where participants conducted a live object recognition study with all 23 objects in five living environments, including a living room, a kitchen, a computer desk with a laptop and monitor, a parking space outside a building, and inside a running car (Subaru Forester) with the radio, heater, and Bluetooth all switched on. The device was powered by a wall outlet when indoor and a battery (floating ground) when outside the building or in a car. The locations were randomized between participants. Within each location, objects were presented in a random order, appearing five times each in total. Real-time prediction results were recorded.
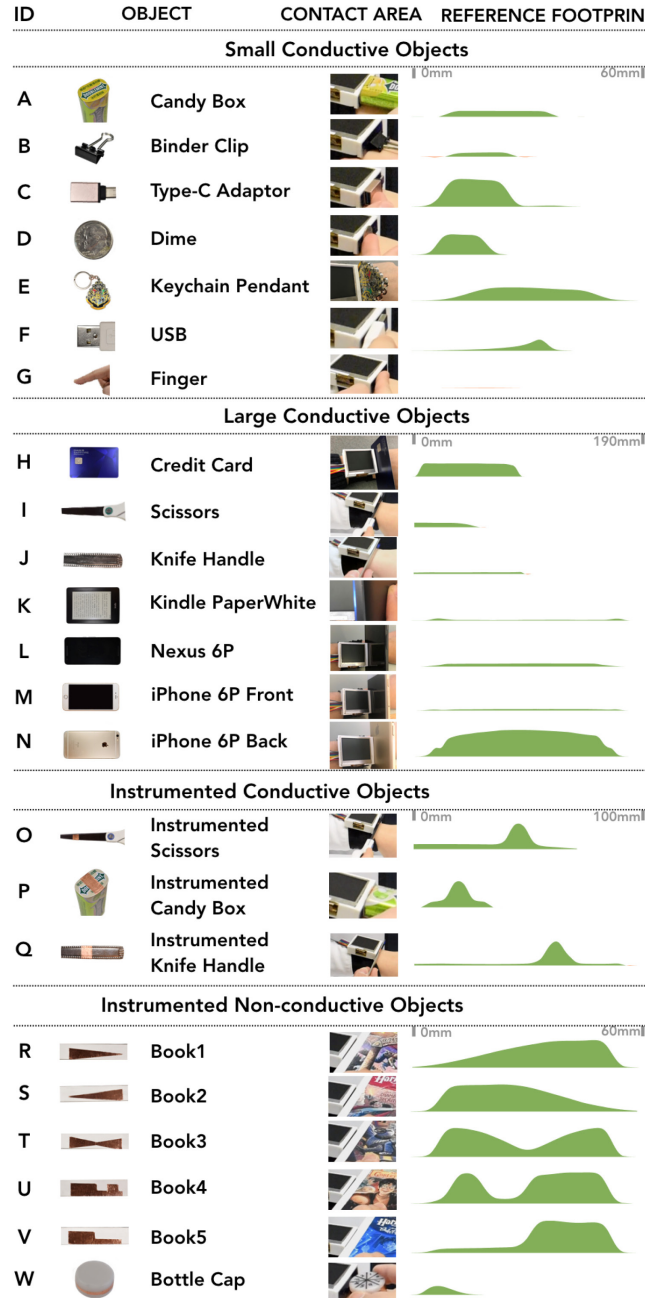

Figure 9. Tested objects shown by type, how they are in contact with the sensor, and their reference footprints (one scan picked randomly from the database).

	A	B	C	D	E	F	G	H	I	J	K	L	M	N	O	P	Q	R	S	T	U	V	W
A	100	0	0	0	0	0	0	0	0	0	0	0	0	0	0	0	0	0	0	0	0	0	0
B	0	100	0	0	0	0	0	0	0	0	0	0	0	0	0	0	0	0	0	0	0	0	0
C	0	0	98	0	0	0	0	0	0	0	0	0	0	0	0	0	0	0	0	0	2	0	0
D	0	0	0	96	0	0	0	0	0	0	0	0	0	0	2	0	0	0	2	0	0	0	0
E	0	0	0	0	100	0	0	0	0	0	0	0	0	0	0	0	0	0	0	0	0	0	0
F	0	2	0	0	0	98	0	0	0	0	0	0	0	0	0	0	0	0	0	0	0	0	0
G	0	0	0	0	0	0	100	0	0	0	0	0	0	0	0	0	0	0	0	0	0	0	0
H	0	0	0	0	6	0	0	94	0	0	0	0	0	0	0	0	0	0	0	0	0	0	0
I	2	0	0	0	0	0	0	0	96	0	0	0	0	0	0	0	0	0	0	0	0	0	0
J	0	0	0	0	0	0	0	0	0	96	0	4	0	0	0	0	0	0	0	0	0	0	0
K	0	0	0	0	0	0	0	0	0	0	92	0	8	0	0	0	0	0	0	0	0	0	0
L	0	0	0	0	0	0	0	0	0	0	0	100	0	0	0	0	0	0	0	0	0	0	0
M	0	0	0	0	0	0	0	0	0	4	0	0	96	0	0	0	0	0	0	0	0	0	0
N	0	0	0	0	0	0	0	0	0	0	0	0	0	98	0	0	0	0	2	0	0	0	0
O	4	0	0	0	0	0	0	0	0	0	0	0	0	0	94	0	2	0	0	0	0	0	0
P	0	0	0	0	0	0	0	0	0	0	0	0	0	0	0	98	2	0	0	0	0	0	0
Q	0	0	0	0	0	0	0	0	0	0	0	0	0	0	0	0	100	0	0	0	0	0	0
R	0	0	0	0	2	0	0	0	0	0	0	0	0	0	0	2	0	94	2	0	0	0	0
S	0	0	0	0	2	0	0	0	2	0	0	0	4	0	0	0	0	0	92	0	0	0	0
T	0	0	0	0	0	0	0	0	0	0	10	0	2	0	0	0	0	0	0	86	0	0	0
U	0	0	0	0	0	2	0	0	0	0	0	0	2	0	0	2	0	0	0	0	92	2	0
V	0	0	6	0	0	0	0	0	2	0	0	0	2	0	0	2	2	0	0	0	0	88	0
W	0	4	0	0	0	0	0	0	0	0	0	0	0	0	0	0	0	0	0	0	0	0	96

Figure 10. Object confusion matrix across 23 objects and 10 participants. Results are shown in percentage.

Result

Our system achieved an overall accuracy of 95.8% (s.e. = 0.81%). Figure 10 shows the confusion matrix for all objects.

Among all tested objects, 21 achieved an accuracy higher than 90%, despite purposeful inclusion of experimental procedures that typically impact recognition accuracy – no per-user calibration, no user training, and considerable time separation between the experiment and when the reference data was collected – which is very promising. We also found that power source (e.g., earth vs floating ground) had a neglectable effect on object recognition. The confusion matrix shows that the Kindle paperwhite (K) was sometimes misclassified as iPhone 6Plus Front (M). This is because both objects have a similar structure with built-in electronic components. Despite the components being different, our sensor was not able to distinguish between them reliably.

The instrumented non-conductive objects were not significantly confused with each other. This is exciting given that the system separated them only using the conductive pattern. Book 3 (T) and Book 5 (V) achieved the lowest accuracy among all the objects, with 86% (s.e. = 4.96%) and 88% (s.e. = 4.64%) accuracy respectively. Book 3 was mostly confused with the Instrumented Scissors (O). As shown in Figure 11 (left), the testing footprint (black dots) can sometimes have shorter distance to the reference footprint of Instrumented Scissors than that of its own. This happens when the book was held with a smaller hinging angle to the sensor, causing the signals to be weak. These types of errors can be mitigated by introducing more weight to the shape of the curve than the distance. Book 5 (V) was occasionally misclassified as a Type-C Adaptor (C). As shown in Figure 11 (right), this is primarily due to the similarity between the reference footprints. This type of error can be solved by using more distinguishable pattern designs.
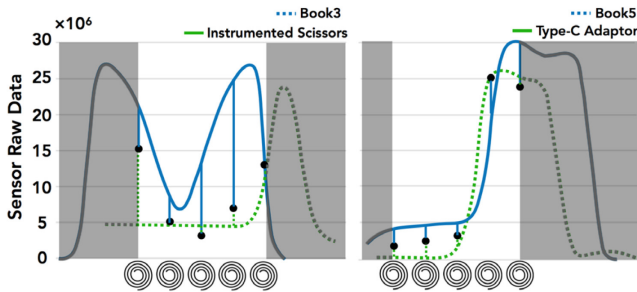

Figure 11. Illustrations of how KNN confused the testing footprints (black dots) with the other objects.

Supplementary Study – Environmental Noise
In principle, our system fails when the background EMI is close to its working frequency (4.63 to 4.94 MHz), which, to the best of our knowledge, is uncommon in daily environments. To investigate the robustness of the system under common environmental noises, we repeated the study with the same set of 23 objects in locations that were within 10cm of a running microwave, WIFI router, and 3D printer. These are common sources of strong electromagnetic noises. With each device, objects were presented in a random order, appearing three times each in total. The study was carried out with a single participant (male, right-handed, 25 years old).

The results showed a real-time recognition accuracy of 100%. We further looked at the raw data and found no significant effect was caused by the tested electromagnetic noises. This again confirms the promise of our approach against common environmental noises.

EVALUATION 2 –1D OBJECT MANIPULATION
The goal of this study was to measure how accurate our system can sense sliding, hinging, and rotation actions. Reference data was collected by the same initial volunteer from our first study, also one week prior to this study. The study was carried out by a single participant (male, right-handed, 21 years old) sitting at a computer desk.

Slide
To measure the sliding accuracy, we randomly picked one object from each category, including *Dime, Credit Card, Instrumented Knife Handle,* and *Book 3*. We also included *Bottle Cap* to investigate the effect of a smaller contact area on tracking accuracy. The study required the participant to wear our device on the wrist of their left hand, and slide each of the objects against the sensor three times. The sliding action needed to be completed from one end (e.g., origin) of the sensor to the other, with an approximate sliding distance of 40 mm. The participant stopped every 2 mm, and the experimenter recorded the ground truth, measured using a ruler mounted against the sensor (Figure 12 right). A computer recorded the predicted distance from the origin.

Results
We used average error distance (ED_{avg}) to measure the sliding accuracy. The ED_{avg} is defined as $\frac{1}{n}\sum_{i=1}^{n}|\hat{y}_i - y_i|$, where $\hat{y}_i$ is predicted location, y_i is ground truth, and n is the number of trials (e.g., 21 locations × 3 repetitions).

The results revealed that the ED_{avg} across all tested objects was less than 1 mm (e.g., 0.82 mm; s.e. = 0.17 mm). Specifically, the average error distance for *Dime, Credit Card, Instrumented Knife Handle*, *Book 3* and *Bottle Cap* are 0.45 mm (s.e. = 0.02 mm), 1.38 mm (s.e. = 0.11 mm), 0.65 mm (s.e. = 0.15 mm), 1.17 mm (s.e. = 0.07 mm) and 0.47 mm (s.e. = 0.07 mm) respectively. Contact size did not affect sliding accuracy, as the *Bottle Cap* received one of the highest accuracies amongst all tested objects. *Book 3* received a relatively low accuracy score. This is due to the imprecision of tracking the valley of the marker. The accuracy for *Credit Card* was also lower than the other tested objects, presumably because of its material. Certainly, more research is needed to investigate how object material may affect the sliding accuracy.
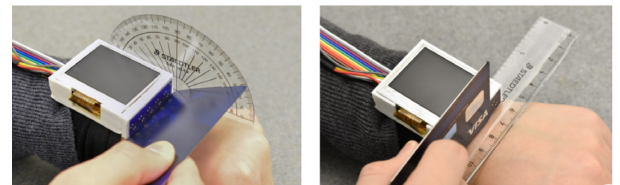

**Figure 12. Study apparatus for hinge (left) and slide (right).**

Hinge

To measure the hinging accuracy, we picked thin, flat objects which included *Credit Card*, *Table Knife*, and *Instrumented Table Knife*. The *Dime* was excluded as it was too small to properly hinge. The *Keychain Pendant* was also excluded due to its uneven contour, as it does not provide a stable hinging axis. During the study, participants hinged open a tested object from 0° to 60° three times and stopped every 4° to allow the experimenter to record the ground truth using a protractor mounted on the watch (Figure 12 left). The predicted hinging angle was also recorded using a computer.

Result

We used average error distance (ED_{avg}) to measure the hinging accuracy. The ED_{avg} is defined as $\frac{1}{n}\sum_{i=1}^{n}|\hat{d}_i - d_i|$, where $\hat{d}_i$ is the predicted hinge degree, d_i is the ground truth, and n is the number of trials (e.g., 16 discrete angles × 3 repetitions).
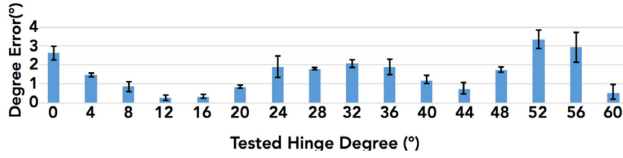
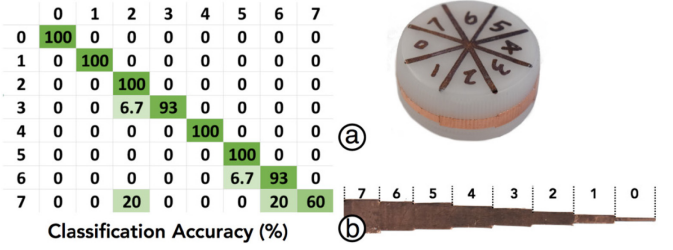**Figure 13. The average error distance of the Credit Card shown by the sample angles.**

The ED_{avg} across all three tested objects was 1.64° (s.e. = 0.37°). Specifically, the average error distance for *Credit Card*, *Knife Handle*, and *Instrumented Knife Handle* were 1.53° (s.e. = 0.13°), 2.48° (s.e. = 0.19°), and 0.92° (s.e. = 0.2°) respectively. The *Instrumented Knife Handle* had the highest accuracy, with its average error distance remaining less than 3°, even up to 80°. Most errors came from the angles away from the ones marked manually, when converting the reference data from the time domain to the hinging angle domain (e.g., 10° and 45°). Figure 13 shows such an example from *Credit Card*. While the accuracy is expected to increase with the increasing number of manually-marked angles, our result is still promising with the least amount of training efforts from a user. Hinging accuracy differed between different objects, also suggesting that more research is required to better understand how object material may affect the sliding accuracy.

Rotation

Rotation was tested with participant rotating the *Bottle Cap* (Figure 14 b) three times at any location inside the sensor. Participant stopped every 9°, and the system recorded the predicted wedge.

Result

The average classification accuracy of the eight wedges was 93% (s.e. = 4.37%). The confusion matrix in Figure 14 shows that most classification errors occurred around the borders of the wedges. Interestingly, Wedge 7 was confused with Wedge 2 for 20% of the time. This is because when the samples were picked from a location closed to the Wedge 1 border, the inductance value got evened to a level similar to

	0	1	2	3	4	5	6	7
0	100	0	0	0	0	0	0	0
1	0	100	0	0	0	0	0	0
2	0	0	100	0	0	0	0	0
3	0	0	6.7	93	0	0	0	0
4	0	0	0	0	100	0	0	0
5	0	0	0	0	0	100	0	0
6	0	0	0	0	0	6.7	93	0
7	0	0	20	0	0	0	20	60

Classification Accuracy (%)

Figure 14. Left: confusion Matrix for the rotation task. Right: the pattern of the conductive marker for the bottle cap.

that of Wedge 2. Similarly, 20% confusion was found between Wedge 7 and Wedge 6 at the border. This is true for the other instances where error occurred and is considered to be acceptable for coarse-grained rotation tasks.

Figure 15. Indutivo demo applications: (a) video player, (b) aircraft game, (c) brick breaker game, (d) audio book app, (e) fitness app, (f) setting voice mode app.

DEMO APPLICATIONS

We implemented six demo applications on a smartwatch to showcase our contact-based sensing technique. Our first application is a video player, which shows Forward, Play/Pause, and Backward buttons on the eastern side of the screen. Tapping a dime on the sensor at the appropriate location near a button, triggers the corresponding action (Figure 15 a). This helps avoid a finger occluding the screen and false input from a hand accidentally touching the sensor. Our second application is a top-down aircraft game. With this game, the instrumented bottle cap can be used to launch the app and as a rotating controller to steer the aircraft (Figure 15 b). Using this approach, the screen space will not be occluded by a controller on the interface or a user's finger. This example shows that a user can use cheap objects and materials to create their own novel smartwatch controllers or input devices. Our third application is a brick breaker game. Like many other games, this game is difficult to play on a smartwatch due to a finger occluding the screen space when dragging a paddle. We show that the paddle can be precisely positioned using a binder clip as a physical handle (Figure 15 c). The fourth application associates a user's books (or associated conductive markers) with audio copies stored on their smartwatch. A user can tap the book on the smartwatch

to play the audio or download it if it doesn't exist on the smartwatch (Figure 15 d). This provides an alternative means to navigating and searching for the desired audio to play. The fifth application is a fitness app, which encourages the user to enter calorie information during a meal. With our app, the user can enter an estimated calorie value by hinging the handle of a table knife, to avoid touching the screen when using a finger that is messy from eating their meal (Figure 15 e). Finally, switching between different modes on a smartwatch can be slow on the current smartwatches. With our last application, a user can use the pendant of their car keys to quickly activate voice mode on the smartwatch before starting a vehicle (Figure 15 f).

LIMITATIONS AND FUTURE WORK

In this section, we discuss the lessons and insights we learned from our experience. We also present limitations of our work and directions for future research.

Contact area. Our current implementation requires objects to be in contact with the sensor, primarily due to the relatively short sensing distance. More investigation and work can be done in increasing the sensing distance since industry (e.g., TI) has shown promising results in achieving a longer range. Ideally, objects can be sensed and manipulated anywhere on the back of the hand, without the need of touching the smartwatch. We expect this to enable many new applications on smartwatches.

Additionally, tapping the object against the sensor allows the contact area to be relatively stable and consistent across different times of use. Objects without a planar contact surface can be challenging to sense because changes in the contact area may affect the inductance footprint. However, this challenge can be overcome with additional reference data since the change in the inductance footprint is consistent with respect to how the object's contact area may change. Similarly, sensing the hinge movement of an object without a stable axis to hinge around (e.g., our keychain pendent) is also possible with better training. The potential tradeoff is that this may introduce confusion between similar objects.

Our sensor works better with objects whose contact area is smaller than the sensor but bigger than a coil because otherwise, the material of an object becomes the primary component to determine recognition capability. Objects that are smaller than the sensor coil can be the most challenging to sense, as the signal can be too small to detect, especially when the object is placed in-between two adjacent coils.

Sensing non-conductive objects. Our method does not work with non-conductive objects without instrumentation. This is a limitation of the induction-based approach. A hybrid approach integrating inductive sensing with the other types of sensing techniques, such as radar-based techniques, is an interesting future direction to explore to come up with a method that can sense both conductive and non-conductive objects and sense their movements.

Interactions. In some smartwatch designs, a knob or button (e.g., digital crown) is placed on the east-facing side of the watch, which conflicts with our sensor placement as well as our interaction techniques. This can be compromised by adjusting the sensor and knob placement or by placing it on different sides of the smartwatch. For example, the interactions could be carried out on the north and south side of the smartwatch, as they are not hindered by the arm or hand. Such sensor placement could create opportunities for new types of interactions that warrant careful future studies.

Beyond smartwatches. Inductive sensing has potential for many other smaller devices like smart bracelets, jewelry, or smart IoTs. For example, different objects can quickly trigger different functions on an Amazon Echo (e.g., tap the book to play the book audio). Users can also quickly switch between different modes of a digital clock and precisely adjust their corresponding values (e.g., set the time) by manipulating the object. Indutivo sensor input could also be integrated into various devices that require security passwords by assigning 1D gestural input with specific conductive objects as a user's password. Further, inductive sensing can also be added on smart rings, supporting contextual input by simply touching different objects. Smart tables could also potentially benefit from this sensing technique by identifying various objects that physically contact it, triggering specific effects (e.g. touching a pen to the table allows a user to draw, touching a brush could trigger painting, etc.). With this type of input, we can save the physical space of buttons or knob on devices and provide richer interactions. Our future investigations will focus on these types of applications and look to overcome challenges on devices that go beyond smartwatches.

CONCLUSION

This paper describes a contact-based, inductive sensing approach to recognize daily conductive objects and sense an object sliding, hinging, and rotating against the sensor. We discuss the sensing principle and present our design of sensor coils to balance sensitivity, sensing range, recognition and tracking accuracy. Through a series of evaluations, we demonstrated that our approach achieved 95.8% real-time classification accuracy with 23 daily objects that included both conductive and non-conductive objects instrumented using low-cost copper tape, as well as a finger. Our approach was also able to sufficiently detect a sliding interaction with an average error distance of 0.82 mm for all objects, a hinge interaction of 1.6° for a credit card, a table knife and an instrumented table knife, and the rotation of an instrumented bottle cap divided into 8 wedges with an accuracy of 93%. The design space of post-touch-screen interaction techniques for small wearables and smart IoTs is broad and requires additional study. Indutivo contributes to this area by enabling users to engage in novel input interactions by detecting, recognizing, and sensing the lateral movement of everyday conductive objects.

REFERENCES

1. Aria Wearable. 2014. Retrieved March 15, 2018 from http://www.ariawearables.com/
2. Samsung Gear Smartwatches. 2018. Retrieved March 11,2018 from https://www.samsung.com/us/mobile/wearables/
3. TI LDC Sensor Design Application Report SNOA930. 2015. Retrieved March 15, 2018 from http://www.ti.com/lit/an/snoa930a/snoa930a.pdf
4. Daniel Ashbrook, Kent Lyons and Thad Starner. 2008. An investigation into round touchscreen wristwatch interaction. In *Proceedings of the 10th International Conference on Human Computer Interaction with Mobile Devices and Services* (MobileHCI'08), 311-314. DOI=http://dx.doi.org/10.1145/1409240.1409276
5. Ling Bao and Stephen S Intille. 2004. Activity recognition from user-annotated acceleration data. In *International Conference on Pervasive Computing* (Pervasive'04), Springer, 1-17. DOI=https://doi.org/10.1007/978-3-540-24646-6_1
6. Eugen Berlin, Jun Liu, Kristof van Laerhoven and Bernt Schiele. 2010. Coming to grips with the objects we grasp: detecting interactions with efficient wrist-worn sensors. In *Proceedings of the fourth international conference on Tangible, embedded, and embodied interaction* (TEI'10), 57-64. DOI=http://dx.doi.org/10.1145/1709886.1709898
7. Michael Buettner, Richa Prasad, Matthai Philipose and David Wetherall. 2009. Recognizing daily activities with RFID-based sensors. In *Proceedings of the 11th international conference on Ubiquitous computing* (UbiComp'09), 51-60. DOI=http://doi.acm.org/10.1145/1620545.1620553
8. Xiang 'Anthony' Chen, Tovi Grossman, Daniel J. Wigdor and George Fitzmaurice. 2014. Duet: exploring joint interactions on a smart phone and a smart watch. In *Proceedings of the SIGCHI Conference on Human Factors in Computing Systems* (CHI'14), 159-168. DOI=https://doi.org/10.1145/2556288.2556955
9. Kai-Yin Cheng, Rong-Hao Liang, Bing-Yu Chen, Rung-Huei Laing and Sy-Yen Kuo. 2010. iCon: utilizing everyday objects as additional, auxiliary and instant tabletop controllers. In *Proceedings of the SIGCHI Conference on Human Factors in Computing Systems* (CHI'10), 1155-1164. DOI=https://doi.org/10.1145/1753326.1753499
10. Artem Dementyev and Joseph A. Paradiso. 2014. WristFlex: low-power gesture input with wrist-worn pressure sensors. In *Proceedings of the 27th annual ACM symposium on User interface software and technology* (UIST'14), 161-166. DOI=https://doi.org/10.1145/1753326.1753499
11. Rui Fukui, Masahiko Watanabe, Tomoaki Gyota, Masamichi Shimosaka and Tomomasa Sato. 2011. Hand shape classification with a wrist contour sensor: development of a prototype device. In *Proceedings of the 13th international conference on Ubiquitous computing* (UbiComp'11), 311-314. DOI=https://doi.org/10.1145/1753326.1753499
12. Jun Gong, Xing-Dong Yang and Pourang Irani. 2016. WristWhirl: One-handed Continuous Smartwatch Input using Wrist Gestures. In *Proceedings of the 29th Annual Symposium on User Interface Software and Technology* (UIST '16), 861-872. DOI=https://doi.org/10.1145/2984511.2984563
13. Tobias Grosse-Puppendahl, Sebastian Herber, Raphael Wimmer, Frank Englert, Sebastian Beck, Julian von Wilmsdorff, Reiner Wichert and Arjan Kuijper. 2014. Capacitive near-field communication for ubiquitous interaction and perception. In *Proceedings of the 2014 ACM International Joint Conference on Pervasive and Ubiquitous Computing* (UbiComp'14), 231-242. DOI=https://doi.org/10.1145/2632048.2632053
14. Gaëtanne Haché, Edward D Lemaire and Natalie Baddour. 2011. Wearable mobility monitoring using a multimedia smartphone platform. In *IEEE transactions on instrumentation and measurement*, 60. DOI=https://doi.org/10.1109/TIM.2011.2122490
15. Chris Harrison and Scott E. Hudson. 2009. Abracadabra: wireless, high-precision, and unpowered finger input for very small mobile devices. In *Proceedings of the 22nd annual ACM symposium on User interface software and technology* (UIST '09), 121-124. DOI=https://doi.org/10.1145/1622176.1622199
16. Chris Harrison, Desney S. Tan and Dan Morris. 2010. Skinput: appropriating the body as an input surface. In *Proceedings of the SIGCHI Conference on Human Factors in Computing Systems* (CHI '10), 453-462. DOI=https://doi.org/10.1145/1753326.1753394
17. Steve Hodges, Alan Thorne, Hugo Mallinson and Christian Floerkemeier. 2007. Assessing and optimizing the range of UHF RFID to enable real-world pervasive computing applications. In *International Conference on Pervasive Computing* (Pervasive'07), 280-297. DOI=https://doi.org/10.1007/978-3-540-72037-9_17
18. Jungsoo Kim, Jiasheng He, Kent Lyons and Thad Starner. 2007. The Gesture Watch: A Wireless Contact-free Gesture based Wrist Interface. In *Proceedings of the 2007 11th IEEE International Symposium on Wearable Computers* (ISWC'07), 1-8. DOI=https://doi.org/10.1109/ISWC.2007.4373770
19. Gierad Laput, Robert Xiao, Xiang 'Anthony' Chen, Scott E. Hudson and Chris Harrison. 2014. Skin buttons: cheap, small, low-powered and clickable fixed-icon laser projectors. In *Proceedings of the 27th annual ACM symposium on User interface software and technology* (UIST'14), 389-394. DOI=https://doi.org/10.1145/2642918.2647356
20. Gierad Laput, Robert Xiao and Chris Harrison. 2016. Viband: High-fidelity bio-acoustic sensing using

commodity smartwatch accelerometers. In *Proceedings of the 29th Annual Symposium on User Interface Software and Technology* (UIST'16), 321-333.
DOI=https://doi.org/10.1145/2984511.2984582

21. Gierad Laput, Chouchang Yang, Robert Xiao, Alanson Sample and Chris Harrison. 2015. Em-sense: Touch recognition of uninstrumented, electrical and electromechanical objects. In *Proceedings of the 28th Annual ACM Symposium on User Interface Software and Technology* (UIST'15), 157-166.
DOI=https://doi.org/10.1145/2807442.2807481

22. Gierad Laput, Chouchang Yang, Robert Xiao, Alanson Sample and Chris Harrison. 2015. Em-sense: Touch recognition of uninstrumented, electrical and electromechanical objects. In *Proceedings of the 28th Annual ACM Symposium on User Interface Software and Technology* (UIST'15), 157-166.
DOI=https://doi.org/10.1145/2807442.2807481

23. Hanchuan Li, Eric Brockmeyer, Elizabeth J. Carter, Josh Fromm, Scott E. Hudson, Shwetak N. Patel and Alanson Sample. 2016. PaperID: A Technique for Drawing Functional Battery-Free Wireless Interfaces on Paper. In *Proceedings of the 2016 CHI Conference on Human Factors in Computing Systems* (CHI'16), 5885-5896.
DOI=https://doi.org/10.1145/2858036.2858249

24. Hanchuan Li, Can Ye and Alanson P. Sample. 2015. IDSense: A Human Object Interaction Detection System Based on Passive UHF RFID. In *Proceedings of the 33rd Annual ACM Conference on Human Factors in Computing Systems* (CHI'15), 2555-2564.
DOI=https://doi.org/10.1145/2702123.2702178

25. Jaime Lien, Nicholas Gillian, M. Emre Karagozler, Patrick Amihood, Carsten Schwesig, Erik Olson, Hakim Raja and Ivan Poupyrev. 2016. Soli: Ubiquitous Gesture Sensing with Millimeter Wave Radar. In *ACM Transactions on Graphics* (SIGGRAPH'16).
DOI=https://doi.org/10.1145/2897824.2925953

26. Takuya Maekawa, Yasue Kishino, Yutaka Yanagisawa and Yasushi Sakurai. 2012. Recognizing handheld electrical device usage with hand-worn coil of wire. In *International Conference on Pervasive Computing* (Pervasive'12), 234-252.
DOI=https://doi.org/10.1007/978-3-642-31205-2_15

27. Jess McIntosh, Asier Marzo and Mike Fraser. 2017. SensIR: Detecting Hand Gestures with a Wearable Bracelet using Infrared Transmission and Reflection. In *Proceedings of the 30th Annual ACM Symposium on User Interface Software and Technology* (UIST'17), 593-597.
DOI=https://doi.org/10.1145/3126594.3126604

28. Norhisam Misron, Loo Qian Ying, Raja Nor Firdaus, Norrimah Abdullah, Nashiren Farzilah Mailah and Hiroyuki Wakiwaka. 2011. Effect of inductive coil shape on sensing performance of linear displacement sensor using thin inductive coil and pattern guide. *Sensors*, 11 (11). 10522-10533.
DOI=https://doi.org/10.3390/s111110522

29. Sunderarajan S Mohan, Maria del Mar Hershenson, Stephen P Boyd and Thomas H Lee. 1999. Simple accurate expressions for planar spiral inductances. *IEEE Journal of solid-state circuits*, 34 (10). 1419-1424.
DOI=https://doi.org/10.1109/4.792620

30. Ian Oakley and Doyoung Lee. 2014. Interaction on the edge: offset sensing for small devices. In *Proceedings of the SIGCHI Conference on Human Factors in Computing Systems* (CHI'14), 169-178.
DOI=https://doi.org/10.1145/2556288.2557138

31. Anke van Oosterhout, Miguel Bruns Alonso, Satu Jumisko-Pyykko. 2018. Ripple Thermostat: Affecting the Emotional Experience through Interactive Force Feedback and Shape Change. In *Proceedings of the SIGCHI Conference on Human Factors in Computing Systems* (CHI'14), 1-12.
DOI=https://doi.org/10.1145/3173574.3174229

32. Santiago Ortega-Avila, Bogdana Rakova, Sajid Sadi and Pranav Mistry. 2015. Non-invasive optical detection of hand gestures. In *Proceedings of the 6th Augmented Human International Conference* (AH'15).
DOI=http://dx.doi.org/10.1145/2735711.2735801

33. Jerome Pasquero, Scott J. Stobbe and Noel Stonehouse. 2011. A haptic wristwatch for eyes-free interactions. In *Proceedings of the SIGCHI Conference on Human Factors in Computing Systems* (CHI'11), 3257-3266.
DOI=https://doi.org/10.1145/1978942.1979425

34. Vesa Peltonen, Juha Tuomi, Anssi Klapuri, Jyri Huopaniemi and Timo Sorsa. 2002. Computational auditory scene recognition. In *IEEE International Conference on Acoustics, Speech, and Signal Processing* (ICASSP'02), II-1941-II-1944.
DOI=https://doi.org/10.1109/ICASSP.2002.5745009

35. Simon T. Perrault, Eric Lecolinet, James Eagan and Yves Guiard. 2013. Watchit: simple gestures and eyes-free interaction for wristwatches and bracelets. In *Proceedings of the SIGCHI Conference on Human Factors in Computing Systems* (CHI'13), 1451-1460.
DOI=https://doi.org/10.1145/2470654.2466192

36. Juhi Ranjan, Yu Yao, Erin Griffiths and Kamin Whitehouse. 2012. Using mid-range RFID for location based activity recognition. In *Proceedings of the 2012 ACM Conference on Ubiquitous Computing* (UbiComp'12), 647-648.
DOI=http://dx.doi.org/10.1145/2370216.2370347

37. Jun Rekimoto. 2001. GestureWrist and GesturePad: Unobtrusive Wearable Interaction Devices. In *Proceedings of the 5th IEEE International Symposium on Wearable Computers* (ISWC'01), 21.
DOI=http://dx.doi.org/10.1109/ISWC.2001.962092

38. Xiaofeng Ren and Matthai Philipose. 2009. Egocentric recognition of handled objects: Benchmark and

analysis. In *Computer Vision and Pattern Recognition Workshops*, 1-8.
DOI=http://dx.doi.org/10.1109/CVPRW.2009.520436

39. Edward Bennett Rosa. 1908. The self and mutual inductances of linear conductors. Bulletin of the Bureau of Standards, Vol. 4, 301-344.

40. T. Scott Saponas, Desney S. Tan, Dan Morris, Ravin Balakrishnan, Jim Turner and James A. Landay. 2009. Enabling always-available input with muscle-computer interfaces. In *Proceedings of the 22nd annual ACM symposium on User interface software and technology* (UIST '09), 167-176.
DOI=https://doi.org/10.1145/1622176.1622208

41. M. Sato, I. Poupyrev and C. Harrison. 2012. Touché: Enhancing Touch Interaction on Humans, Screens, Liquids, and EverydayObjects. In *Proceedings of the SIGCHI Conference on Human Factors in Computing Systems* (CHI '12), 483-492.
DOI=http://dx.doi.org/10.1145/2207676.220774

42. Teddy Seyed, Xing-Dong Yang and Daniel Vogel. 2016. Doppio: A Reconfigurable Dual-Face Smartwatch for Tangible Interaction. In *Proceedings of the 2016 CHI Conference on Human Factors in Computing Systems* (CHI'16), 4675-4686.
DOI=https://doi.org/10.1145/2858036.2858256

43. Joshua R Smith, Kenneth P Fishkin, Bing Jiang, Alexander Mamishev, Matthai Philipose, Adam D Rea, Sumit Roy and Kishore Sundara-Rajan. 2005. RFID-based techniques for human-activity detection. *Communications of the ACM*, 48 (9). 39-44.
DOI=http://dx.doi.org/10.1145/1081992.1082018

44. Nicolas Villar, Daniel Cletheroe, Greg Saul, Christian Holz, Tim Regan, Oscar Salandin, Misha Sra, Hui-Shyong Yeo, William Field and Haiyan Zhang. 2018. Project Zanzibar: A Portable and Flexible Tangible Interaction Platform. In *Proceedings of the 2018 CHI Conference on Human Factors in Computing Systems.*
DOI=https://doi.org/10.1145/3173574.3174089

45. Edward J Wang, Tien-Jui Lee, Alex Mariakakis, Mayank Goel, Sidhant Gupta and Shwetak N Patel. 2015. Magnifisense: Inferring device interaction using wrist-worn passive magneto-inductive sensors. In *Proceedings of the 2015 ACM International Joint Conference on Pervasive and Ubiquitous Computing* (UbiComp'15), 15-26.
DOI=https://doi.org/10.1145/2750858.2804271

46. Jamie A Ward, Paul Lukowicz, Gerhard Troster and Thad E Starner. 2006. Activity recognition of assembly tasks using body-worn microphones and accelerometers. *IEEE transactions on pattern analysis and machine intelligence*, 28 (10). 1553-1567.
DOI=https://doi.org/10.1109/TPAMI.2006.197

47. Robert Xiao, Teng Cao, Ning Guo, Jun Zhuo, Yang Zhang and Chris Harrison. 2018. LumiWatch: On-Arm Projected Graphics and Touch Input. In *Proceedings of the 2018 CHI Conference on Human Factors in Computing Systems* (CHI '18).
DOI=https://doi.org/10.1145/3173574.3173669

48. Robert Xiao, Gierad Laput and Chris Harrison. 2014. Expanding the input expressivity of smartwatches with mechanical pan, twist, tilt and click. In *Proceedings of the SIGCHI Conference on Human Factors in Computing Systems* (CHI'14), 193-196.
DOI=https://doi.org/10.1145/2556288.2557017

49. Robert Xiao, Gierad Laput, Yang Zhang and Chris Harrison. 2017. Deus EM Machina: on-touch contextual functionality for smart IoT appliances. In *Proceedings of the 2017 CHI Conference on Human Factors in Computing Systems* (CHI'17), 4000-4008.
DOI=https://doi.org/10.1145/3025453.3025828

50. Rayoung Yang and Mark W. Newman. 2013. Learning from a learning thermostat: lessons for intelligent systems for the home. In *Proceedings of the 2013 ACM international joint conference on Pervasive and ubiquitous computing* (UbiComp'13), 93-102.
DOI=https://doi.org/10.1145/2493432.2493489

51. Hui-Shyong Yeo, Gergely Flamich, Patrick Schrempf, David Harris-Birtill and Aaron Quigley. 2016. Radarcat: Radar categorization for input and interaction. In *Proceedings of the 29th Annual Symposium on User Interface Software and Technology* (UIST'16), 833-841.
DOI=https://doi.org/10.1145/2984511.2984515

52. Yang Zhang and Chris Harrison. 2015. Tomo: Wearable, Low-Cost Electrical Impedance Tomography for Hand Gesture Recognition. In *Proceedings of the 28th Annual ACM Symposium on User Interface Software and Technology* (UIST'15), 167-173.
DOI=https://doi.org/10.1145/2807442.2807480

53. Yang Zhang, Robert Xiao and Chris Harrison. 2016. Advancing hand gesture recognition with high resolution electrical impedance tomography. In *Proceedings of the 29th Annual Symposium on User Interface Software and Technology* (UIST'16), 843.
DOI=https://doi.org/10.1145/2984511.2984574

54. Yang Zhang, Junhan Zhou, Gierad Laput and Chris Harrison. 2016. SkinTrack: Using the Body as an Electrical Waveguide for Continuous Finger Tracking on the Skin. In *Proceedings of the 2016 CHI Conference on Human Factors in Computing Systems* (CHI'16), 1491-1503.
DOI=https://doi.org/10.1145/2984511.2984574

55. Jonsenser Zhao. 2010. A new calculation for designing multilayer planar spiral inductors. EDN (Electrical Design News), 55 (14). 37.

56. Junhan Zhou, Yang Zhang, Gierad Laput and Chris Harrison. 2016. AuraSense: enabling expressive around-smartwatch interactions with electric field sensing. In *Proceedings of the 29th Annual Symposium on User Interface Software and Technology (UIST'16)*, 81-86.
DOI=https://doi.org/10.1145/2984511.2984568